

FRACTURE BEHAVIOUR OF HISTORIC OAK WOOD

Rianne A. Luimes¹, Akke S.J. Suiker², Henk L. Schellen³, André J.M. Jorissen⁴

ABSTRACT: Damage that might originate from climate fluctuations can be observed on decorated oak wooden panels in historical Dutch cabinets and panel paintings. A thorough analysis of the damage mechanisms is needed to obtain a comprehensive understanding of the causes of damage and to develop sustainable conservation strategies. For this purpose, the combined experimental and numerical characterisation of the fracture behaviour of historic and new oak wood is studied. Three point-bending tests are performed, and the measured failure responses and fracture paths are compared against results computed with a finite element model, in which discrete fracture behaviour is simulated with an interface damage model. The experimental and numerical results are in good agreement. The experiments show a quasi-brittle fracture response for the oldest samples and a more brittle fracture response for the new samples. In addition, the strength required for crack initiation along a radial-longitudinal fracture plane is higher than for a tangential-longitudinal fracture plane and the strength depends on the specimen size. Photographs and scanning electron microscopy photos illustrate that fibre bridging is more apparent for the oldest samples, and that the location of crack initiation is set by geometrical imperfections. Moreover, differences in density characterize the crack propagation path.

KEYWORDS: Oak wood, Three-point bending, Fracture toughness, Discrete fracture, Interface damage model

1 INTRODUCTION

Decorated oak wooden panels in historical Dutch cabinets and panel paintings occasionally show damage that might originate from thermal and hygral climate fluctuations. To preserve these highly valuable and susceptible museum objects for future generations, preeminent museums apply severe preservation strategies. Strict standards for indoor climate conditions are followed by imposing strong limitations on indoor temperature and relative humidity fluctuations. This results in a low risk preservation of susceptible museum objects, though at the expense of high energy demands and costs of large heating, ventilating and air conditioning (HVAC) systems. The understanding of the origin of damage and the possible harmful effects of climate fluctuations is essential for improving future preservation strategies.

Recently, decorated oak wooden panels were extensively analysed to characterize these objects in full detail [1]. Relevant empirical data, including aspects like method of construction, conservation treatments and damage occurrence due to climate fluctuations, was collected from a large group of naturally-aged museum objects consisting of 138 doors of 70 Dutch cabinets and 254 Dutch panel paintings. All panels were composed of high quality radial cut oak wooden boards, where the top layers were made of a variety of wood species or a combination of ground and paint layers. It was observed that shrinkage of approximately 1% of the original panel width is dominant in the radial material direction, and that visible cracks, when present, were mainly located along the wood grain direction. In addition, substantial glue-joint failure was observed at connections between the oak wood boards.

Advanced numerical models that can accurately simulate climate-induced damage development in decorated oak wooden panels, in combination with experimental tests and microscopy analyses of the oak wood cellular microstructure, can further improve the understanding and interpretation of these in-situ observations. The present paper presents a first step in this direction by focussing on the experimental-numerical characterisation of the discrete fracture behaviour of historic and new oak wood induced by mechanical loading. Three-point bending tests were performed to analyse the failure response and corresponding fracture path. Scanning

¹ Rianne A. Luimes, Eindhoven University of Technology, The Built Environment, P.O. Box 513, 5600 MB Eindhoven, The Netherlands, r.a.luimes@tue.nl

² Akke S.J. Suiker, Eindhoven University of Technology, The Built Environment, P.O. Box 513, 5600 MB Eindhoven, The Netherlands, a.s.j.suiker@tue.nl

³ Henk L. Schellen, Eindhoven University of Technology, The Built Environment, P.O. Box 513, 5600 MB Eindhoven, The Netherlands, h.l.schellen@tue.nl

⁴ André J.M. Jorissen, Eindhoven University of Technology, The Built Environment, P.O. Box 513, 5600 MB Eindhoven, The Netherlands, a.j.m.jorissen@tue.nl

electron microscopy was used to study the microstructure at the fracture plane. For modelling discrete fracture, the continuum elements in the finite element method (FEM) model are surrounded by interface elements equipped with the mixed-mode interface damage model presented in [2]. This approach was originally proposed in [3], and allows for the description of complex cracking paths in arbitrary directions, including the effects of crack bifurcation and coalescence. To the authors' knowledge this modelling strategy has not been used previously for the simulation of discrete fracture behaviour in wood; instead various other strategies were applied, see [4-6].

The paper is organized as follows: Section 2 describes the test samples, the loading conditions for the three-point bending tests and the determination of the ultimate load and fracture toughness. Section 3 discusses the experimental results in terms of the load-displacement response, the fracture path, and the microstructure at the fracture plane. The discrete fracture model is described in Section 4 and the numerical results are discussed in Section 5. Section 6 outlines the main conclusions.

2 EXPERIMENTAL TESTS

The analysis of naturally-aged museum objects illustrates that decorated oak wooden panels show damage predominantly in the directions perpendicular to the wood grain direction [1]. In correspondence with these observations, in the present study the fracture behaviour of historic oak wood is analysed for cracks running along the wood grain direction, i.e., the longitudinal direction, with the crack plane normal oriented in the tangential direction (TL cracks) or in the radial direction (RL cracks). The fracture behaviour is characterized in terms of the load-displacement response, fracture toughness, ultimate load, fracture path and the microstructure at the fracture plane. The fracture properties measured are used for calibrating and validating the interface damage model used in the present study, see [2] and Section 4 for more details.

2.1 TEST SAMPLES

In accordance with [7], the test specimens were composed of two supporting beams sandwiching a square block, see Figure 1. The bonds were made with a PVA glue (NOVA COL D2 A). The square block was equipped with a notch to ensure crack propagation at the centre of the specimen along the TL or RL material directions. The beams were made of new oak wood and the square block at the centre of the specimen was made of either historic oak wood, dated 1300 A.D. or 1668 A.D., or new wood. The historic oak wood was provided by the Agency for Palaces and Cultural Properties in Denmark and the National Museum of Denmark. Archival sources and building archaeology were considered to determine the date of origin. Two different samples sizes were selected, which are both representative for the dimensions of museum objects [1].

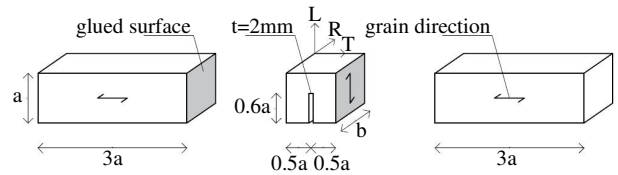


Figure 1: Geometry and dimensions of the test samples. The longitudinal, radial and tangential directions are indicated by the letters L, R and T, respectively.

Relatively large samples with a length and height of $a=45\text{mm}$ and a width of $b=30\text{mm}$ and relatively small samples with $a=25\text{mm}$ and $b=20\text{mm}$ were tested. For the specimens containing a historic oak wooden square block with a TL crack, both large and small samples were tested, and for the specimens containing a block with an RL crack only the small sample was tested. For the specimens completely composed of new oak wood and containing a TL or RL crack, both the large and small samples were tested. The length of the central notch was $0.6a$ and the length of the supporting beams was $3a$. Each specific specimen configuration was tested 5 to 7 times in order to check the repeatability of the experiment and to determine the spread in the test results.

2.2 SAMPLE PREPARATION

Prior to testing, all test specimens were prepared according to a step-wise procedure. First, the beams and square block were put in a climate chamber at a temperature of 20°C and a relative humidity of 60%. When the equilibrium moisture content (EMC) was reached (at which the sample weight remains constant over time), the components were bonded together with a PVE glue. After the curing process of the glue was finished, the test specimen was taken out of the climate chamber. Subsequently, a central notch was applied, where the shape of the notch tip was made by using a blunt saw and a file. As a next step, a three-point bending test was performed. After the test was finished, the EMC of the square block was determined for which the mass at 60% relative humidity and the oven dry mass was measured of a small part taken from the square block [8]. The average EMC for all specimen configurations ranged between 10.4% and 15.0%.

2.3 EXPERIMENTAL SETUP

The experimental set-up shown in Figure 2 meets the requirements described in [7]. The test specimen is simply-supported, where the supports are composed of a solid steel L-shaped plate and a solid steel cylinder. The quasi-static load is applied in a displacement-controlled fashion at the mid-span of the specimen, via a steel plate with a rounded edge. For the small and large test samples the loading rate equals 0.4mm/min and 0.6mm/min , respectively. The magnitude of the load is measured by a load cell and the corresponding displacement is measured through a linear variable displacement transducer (LVDT).

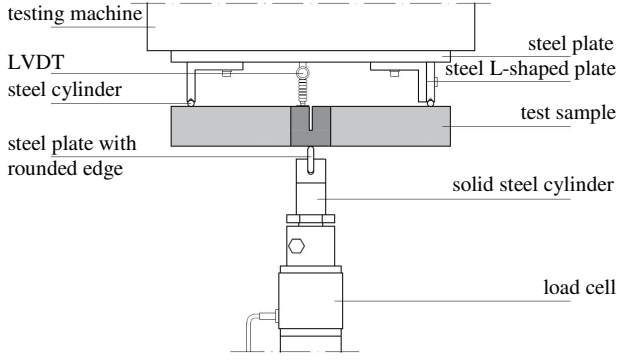


Figure 2: Experimental set-up.

2.4 PARAMETERS

The failure response obtained under three-point bending allows for the determination of the fracture toughness and ultimate load. The fracture toughness of the test specimen is characterized by the area under the load-displacement curve divided by the fracture surface, i.e.,

$$G_f = \frac{1}{A} \int_0^w F(w) dw, \quad (1)$$

where F is the applied load, w is the displacement, and A is the fracture surface. The failure load F_{max} is defined as the maximal load.

3 EXPERIMENTAL RESULTS

Figures 3, 4 and 5 depict the applied load F versus the displacement w for, respectively, the historic oak wood dated 1300 A.D. and 1668 A.D. and the new oak wood. The corresponding failure responses of the small sample with the TL crack are depicted in Figures 3a, 4a and 5a, the responses of the large sample with the TL crack are illustrated in Figures 3b, 4b and 5b, the responses of the small sample with the RL crack are shown in Figures 3c, 4c and 5c, and the response of the large sample with the RL crack is illustrated in Figure 5d. For all samples the load initially increases approximately linearly with increasing displacement, representing an elastic response. After reaching the peak strength, the failure process develops, whereby different failure responses can be observed for the historic and new samples. For the historic samples dated 1300 A.D., the load monotonically decreases with increasing displacement, in correspondence with the initiation of a macroscopic failure crack. This softening process continues until the load has dropped to zero and the failure crack has mobilised across the complete specimen height. For the historic samples dated 1668 A.D., a sudden dynamic drop in load can be observed during which the displacement remains virtually constant. This drop in load is caused by the fact that a quasi-static response here would be characterised by a so-called “snap-back behaviour”, where during failure a decrease in load magnitude is accompanied by a decrease in beam displacement. This essentially indicates that the energy incrementally dissipated by the relatively brittle failure crack is lower than the energy incrementally released

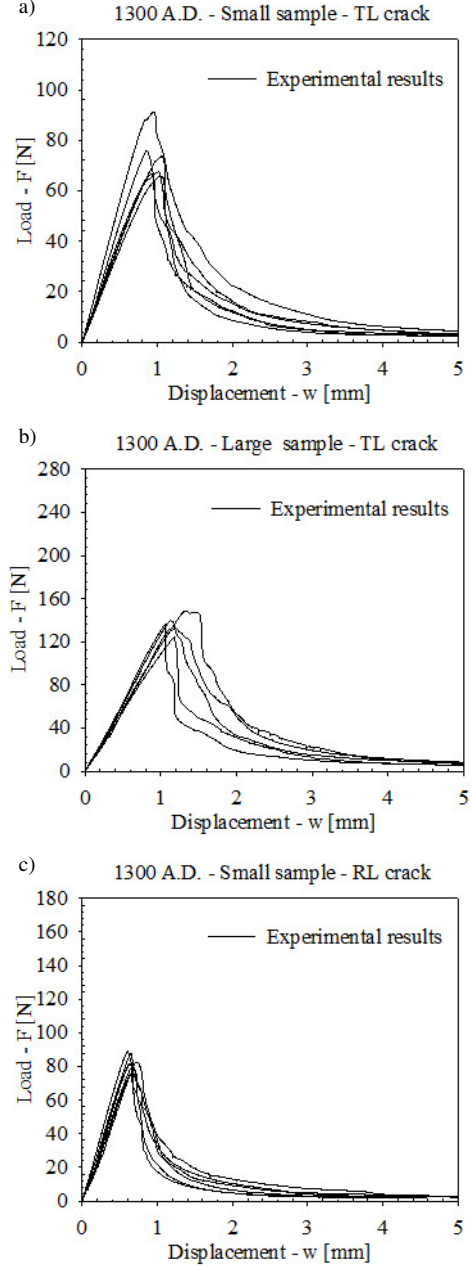


Figure 3: Experimental load-displacement curves for historic oak wooden beams dated 1300 A.D. under 3-point bending. a) Small sample with a TL crack. b) Large sample with a TL crack. c) Small sample with an RL crack.

during elastic unloading in the two adjacent beam parts. Since the three-point bending test is performed in a displacement-controlled fashion, such a snap-back behaviour cannot be followed, and therefore results in an abrupt dynamic decrease in load. Observe, though, that in most cases the measured load signal does not straightforwardly drop to zero; instead, it picks up the quasi-static failure response at a relatively low load level and continues to follow the corresponding softening branch under increasing displacement, until the specimen is completely broken. The failure response of the new samples and historic samples dated 1668 A.D. is comparable, although for the new samples the abrupt dynamic drop in load is somewhat larger. In summary, from the measured failure responses a distinction can be

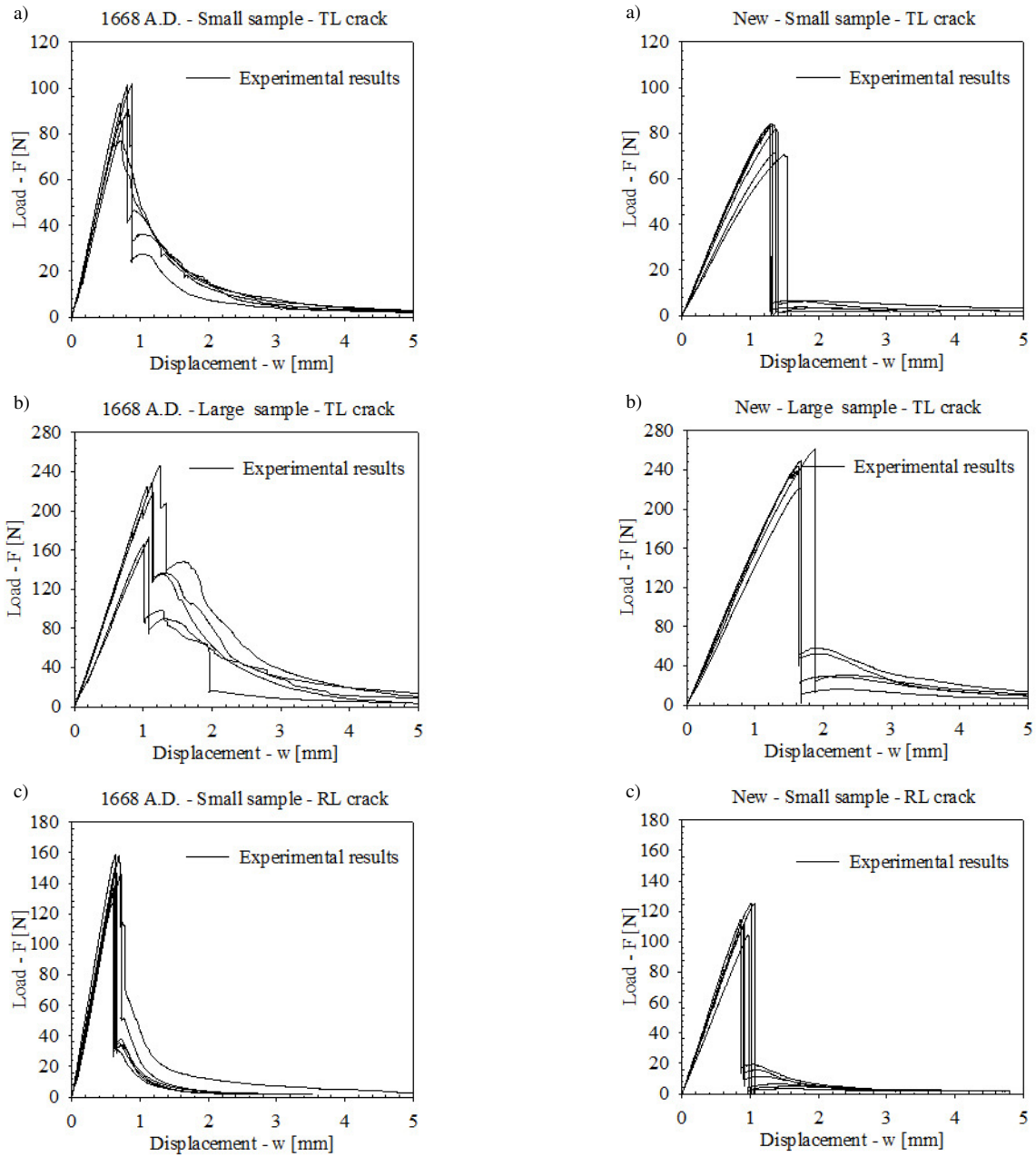


Figure 4: Experimental load-displacement curves for historic oak wooden beams dated 1668 A.D. under 3-point bending. a) Small sample with a TL crack. b) Large sample with a TL crack. c) Small sample with an RL crack.

made between a quasi-brittle fracture response measured for the oldest wood and a considerably more brittle fracture response measured for the wood dated 1668 A.D. and the new wood. The effect on the failure characteristics by the sample size and the orientation of the crack with respect to the material direction will be discussed in more detail in Section 3.4.

3.1 FRACTURE PATH

The fracture path of a small sample dated 1300 A.D. and experiencing a TL crack is illustrated in Figure 6. This fracture path appears to be representative of all specimen configurations tested. The crack nucleates at the right side of the notch (Figure 6b), and subsequently develops along an approximately straight trajectory (Figure 6c).

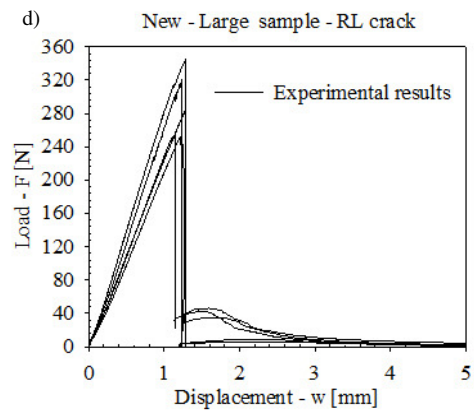


Figure 5: Experimental load-displacement curves for new oak wooden beams under 3-point bending. a) Small sample with a TL crack. b) Large sample with a TL crack. c) Small sample with an RL crack. d) Large sample with an RL crack.

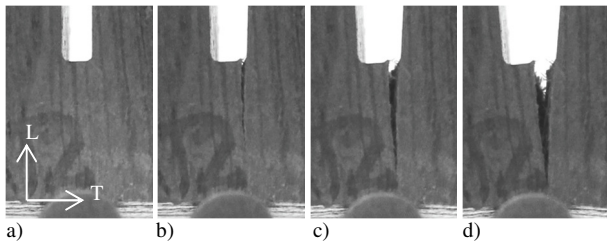


Figure 6: Fracture path of a small historical test sample dated 1300 A.D. with a TL crack. a) Elastic response. b) Crack initiation. c) Crack propagation. d) Ultimate failure.

The resistance against fracture is governed by cell material bridging the crack faces, which, once broken, delaminated or pulled-out, precludes the ultimate failure of the sample (Figure 6d). The bridging of cells is especially apparent for the historical samples dated 1300 A.D., as can be observed from the failure crack of the historical and new samples, see Figure 7. This results in a less brittle response than for the samples dated 1668 A.D. and the new samples, see Figures 4 and 5.

3.2 CRACK INITIATION AND PROPAGATION

From Figure 7 it can be noticed that the location of the initial crack may vary, since small geometrical irregularities at the notch tip trigger the specific location of crack initiation. Nonetheless, the experimental results depicted in Figures 3, 4, and 5 and the computational results presented in Section 5 indicate that the presence of an initial imperfection only has a small influence on the overall failure response. Further, the undulations of the generated crack faces are determined by the differences in material density originating from the oak wood growth process, where the large thin-walled cells (vessels) and thin-walled fibres characterize a low-density early wood while high-density late wood is characterized by small thick-walled cells and thick-walled fibres, see Figure 8. The undulated crack trajectory is most pronounced for the historical samples dated 1300 A.D. depicted in Figures 8c and 8d. Since these undulations increase the area of the fracture surface, they result in a less brittle fracture behaviour, as observed for this historical wood in Figure 3.

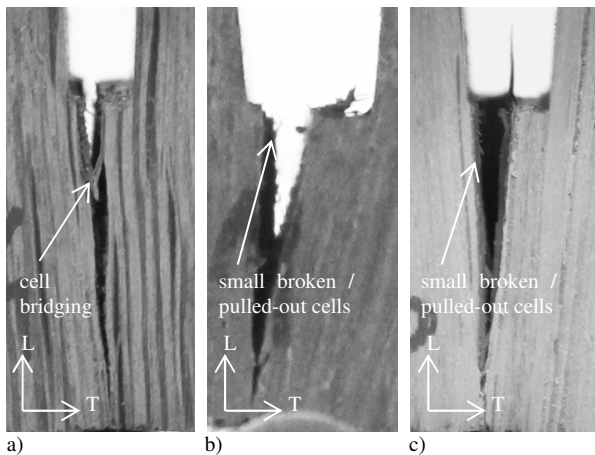


Figure 7: Fracture path at ultimate failure. a) Historical sample dated 1300 A.D. b) Historical sample dated 1668 A.D. c) New sample.

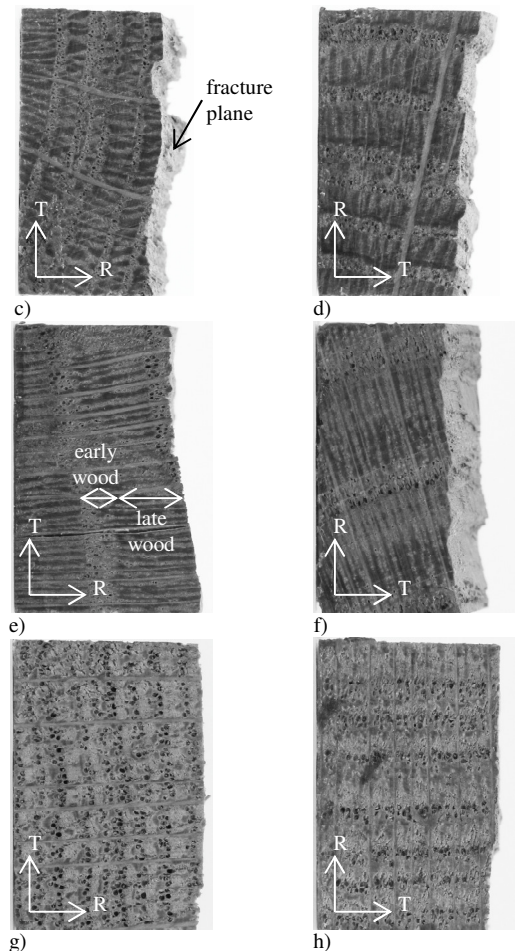
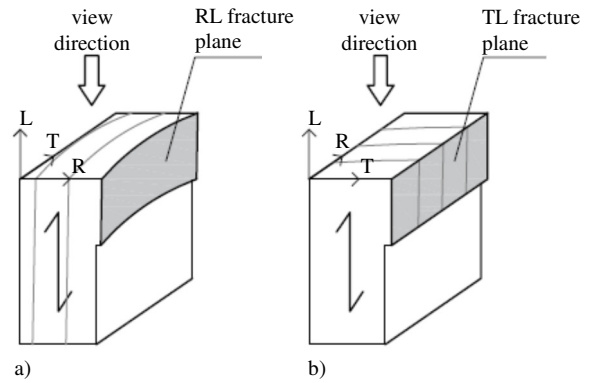


Figure 8: Top view of the historical and new samples. a) View direction for a sample with an RL crack. b) View direction for a sample with a TL crack. c) Historical sample dated 1300 A.D. with an RL crack. d) Historical sample dated 1300 A.D. with a TL crack. e) Historical sample dated 1668 A.D. with an RL crack. f) Historical sample dated 1668 A.D. with a TL crack. g) New sample with an RL crack. h) New sample with a TL crack.

3.3 OAK WOOD MICROSTRUCTURE

The microstructures of the fracture planes of small historical and new oak wood samples are represented in the scanning electron microscopy photographs, see Figures 9 and 10. Typical oak wood cell types can be observed, such as large early wood vessels, small late wood vessels, vessel tracheids, longitudinal parenchyma cells, horizontal small and large parenchyma ray cells,

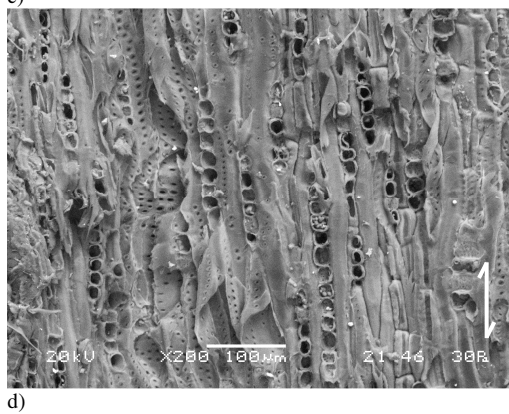
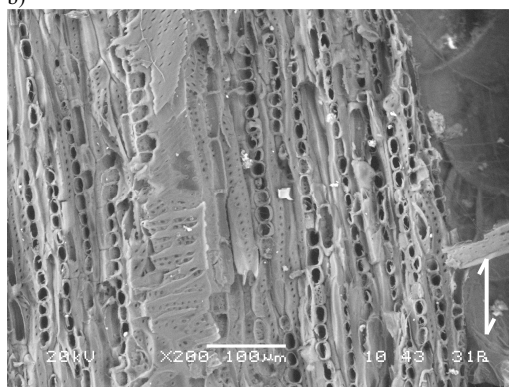
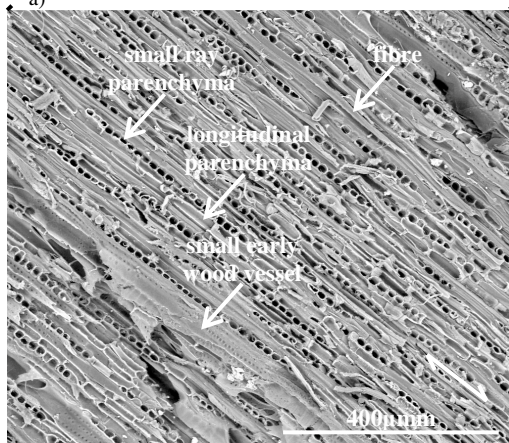
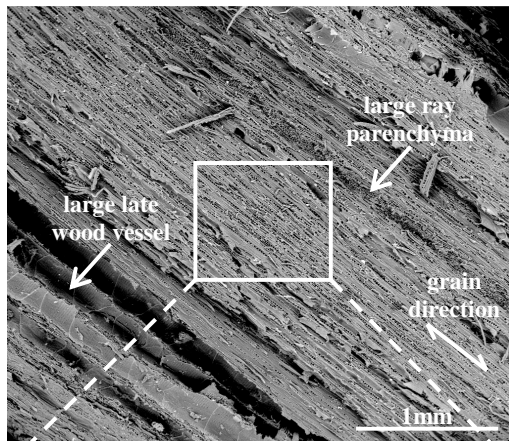


Figure 9: Microstructure at the RL fracture plane. a) Historical sample dated 1300 A.D., 34 times magnification. b) Historical sample dated 1300 A.D., 131 times magnification. c) Historical sample dated 1668 A.D., 200 times magnification. d) New sample, 200 times magnification.

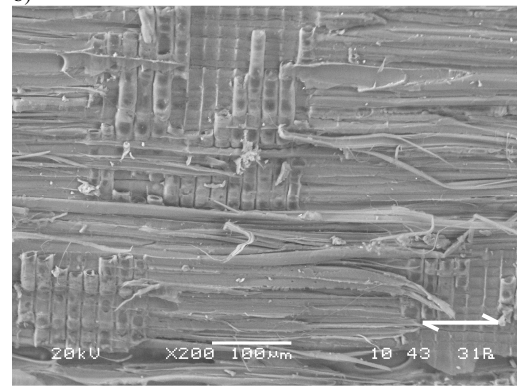
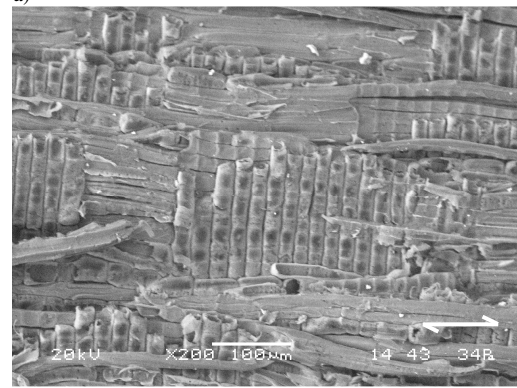
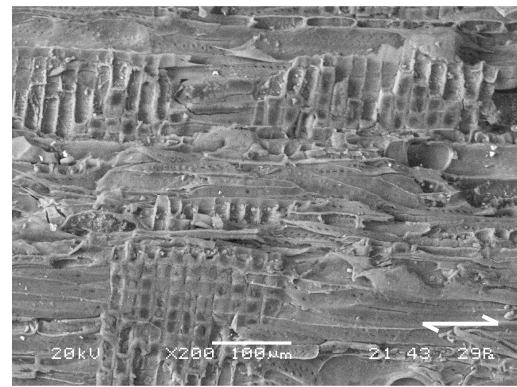


Figure 10: Microstructure at the TL fracture plane. a) Historical sample dated 1300 A.D., 200 times magnification. c) Historical sample dated 1668 A.D., 200 times magnification. d) New sample, 200 times magnification.

thinner-walled early wood fibres and thick-walled late wood fibres. The failure behaviour of these cells characterizes the overall fracture resistance and failure response of the sample along the TL and RL fracture planes, although it is difficult to establish this relation more quantitatively. The vessels and parenchyma cells show mainly trans-wall fracture and the fibres show inter-cell failure, i.e., delamination. Besides, at the TL fracture plane, inter-cell delamination can be observed along the interfaces between rays and fibres and/or rays and longitudinal parenchyma. For the historical wood the number of rays is larger than for the new wood. Additionally, the historical wood has a lower number of fibres and longitudinal parenchyma cells.

Table 1: Fracture toughness G_f and failure load F_{max} following from the experiments. The parameters μ and σ respectively represent the average value and the standard deviation over the number of tested samples of a specific date of origin, specimen size and fracture plane.

| Sample | | | G_f [N/mm] | | F_{max} [N] | |
|----------------------|-------|----------|--------------|------------|---------------|------------|
| | | | μ_G | σ_G | μ_F | σ_F |
| Historical 1300 A.D. | Small | TL crack | 0.47 | 0.10 | 73.5 | 9.64 |
| | | RL crack | 0.36 | 0.07 | 82.6 | 5.09 |
| | Large | TL crack | 0.35 | 0.07 | 136 | 8.99 |
| Historical 1668 A.D. | Small | TL crack | 0.46 | 0.05 | 92.8 | 10.0 |
| | | RL crack | 0.38 | 0.11 | 148 | 11.6 |
| | Large | TL crack | 0.51 | 0.13 | 207 | 35.2 |
| New | Small | TL crack | 0.34 | 0.05 | 79.9 | 6.11 |
| | | RL crack | 0.35 | 0.04 | 115 | 8.29 |
| | Large | TL crack | 0.59 | 0.08 | 243 | 14.8 |
| | | RL crack | 0.42 | 0.04 | 292 | 41.2 |

3.4 FRACTURE TOUGHNESS AND FAILURE LOAD

From the load-displacement curves in Figures 3, 4, and 5, the failure load F_{max} was determined and the fracture toughness G_f was calculated in accordance with Eq. (1). The average value and the standard deviation of these two parameters are listed in Table 1. Both for the historical and new samples a general trend for the fracture toughness G_f in terms of date of origin, specimen size or fracture plane could not be deduced. Although the standard deviation of the fracture toughness is about 20% of the corresponding average value for all specific configurations tested, which seems reasonable for oak wood, aspects like place of origin, forest density, local climate conditions, etc. likely are the reason for causing a significant spread in the overall test results. For the historical and new samples with an RL crack the ultimate load is 12% to 59% higher than for the corresponding samples with a TL crack. However, a general trend in terms of date of origin or specimen size cannot be established, for similar reasons as mentioned above.

4 NUMERICAL MODEL

The fracture responses obtained from the experimental tests outlined in Section 3 are simulated numerically by using the finite element program ABAQUS [9]. To allow for the modelling of cracking paths in arbitrary directions, the finite element model is composed of interface elements surrounding continuum elements, where the interface damage model presented in [2] is adopted for the interface elements and a linear elastic material model is used for the continuum elements. This modelling approach was originally proposed in [3] and has been successfully applied in failure analyses of various engineering materials [10-12]. The interface damage model uses a linear traction-separation law, where the fracture toughness is based on a mode-mixity criterion commonly used for describing brittle interfacial fracture. The numerical implementation is based on an implicit (backward) Euler scheme together with a consistent tangent operator. The interface damage model is incorporated in ABAQUS by using the user-supplied subroutine (UMAT) option. More details on the geometry and boundary conditions of the finite element

model, the finite element discretisation and the material properties can be found in [13].

5 NUMERICAL RESULTS

Figure 11 depicts the load F versus the displacement w for the small sample dated 1300 A.D. that experiences a TL crack. The simulated failure behaviour of the large sample with a TL crack and the small sample with the RL crack of the historic oak wood dated 1300 A.D. have been omitted here, but can be found in [13]. Further, the simulations for the historic oak wood dated 1668 A.D. and new oak wood are currently in development and the results will be published in a forthcoming publication. Observe from Figure 11 that the introduction of a geometrical imperfection at the top of the notch decreases the failure load by approximately 6%. In addition, the failure load and fracture toughness for the isotropic elastic model are 5% to 13% smaller than those for the orthotropic elastic model. The failure load and fracture toughness of the experiments and simulations are in close agreement, see reference [13] for a more detailed comparison. For reaching this level of correspondence, however, the fracture toughness and strength parameters used in the interface damage model for the large sample had to be taken smaller than for the small sample. This difference can be motivated from a so-called “statistical size effect”, which states that the chance of meeting weak inhomogeneities/imperfections during crack propagation for a large sample is higher (since more material points need to be broken for creating the failure crack, which increases the statistical sample size) than for a small sample [14]. Accordingly, the (average) strength and toughness values measured for a large sample typically are smaller than for a small sample. Since oak wood has a rather inhomogeneous material structure (e.g., annular rings of several mm’s in thickness), it can be expected that the spatial variation in the local mechanical properties is significant. Obviously, the statistical size effect following from such inhomogeneities is neglected in numerical simulations when assuming a homogeneous material characterized by specific material parameters. Conversely, the so-called “mechanical size effect” is adequately accounted for in the current numerical simulations. This size effect refers to a sample size-dependency of the measured

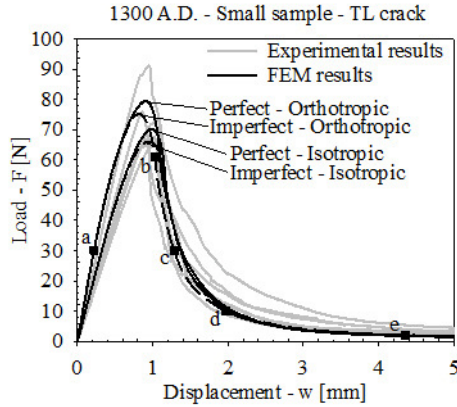


Figure 11: Load-displacement curves for historic oak wooden beams dated 1300 A.D. under three-point bending; FEM results (black lines) versus the experimental results taken from Figure 3 (grey lines). The characters a,b,c,d,e represent the 5 states at which the fracture path is considered in Figure 12.

strength and toughness values as a result of the mechanical response being characterized by length scales following from the fracture process (i.e., crack length, fracture process zone) and length scales defining the structural geometry (i.e., the specimen dimensions). Here, the contribution by the relative crack length to the energetic size effect is automatically accounted for by using a discrete fracture approach, while the influence by the fracture process zone is incorporated by means of the softening characteristics adopted in the interface damage model.

Figure 12 illustrates the numerical fracture path for the small sample with the TL crack. By comparing Figure 12 to Figure 6, it can be concluded that the numerical fracture path is in good correspondence with the experimental fracture path. Note that there is a small difference in the precise location of crack initiation. In the numerical simulation this location is set by a small geometrical imperfection that mimics the effect of local irregularities present at the notch tip. However, as already mentioned, the influence of the precise location of the imperfection on the characteristics of the failure response is negligible.

6 CONCLUSIONS

The fracture behaviour of historic and new oak wood is analysed by means of experimental tests and numerical simulations. The (quasi-)brittle failure response is characterised and the corresponding fracture pattern is determined. The interface damage model adopted from [2] shows to be capable to accurately simulate the experimental failure behaviour. In future work a dissipation-based path-following solution method will be implemented to allow for the robust simulation of brittle failure responses with snap-back behaviour, as relevant for the brittle historical oak wood dated 1668 A.D. and the new oak wood. This model will also be combined with a multi-physics model, in order to simulate the climate-induced damage observed in decorated oak wooden panels in historical Dutch cabinets and panel paintings.

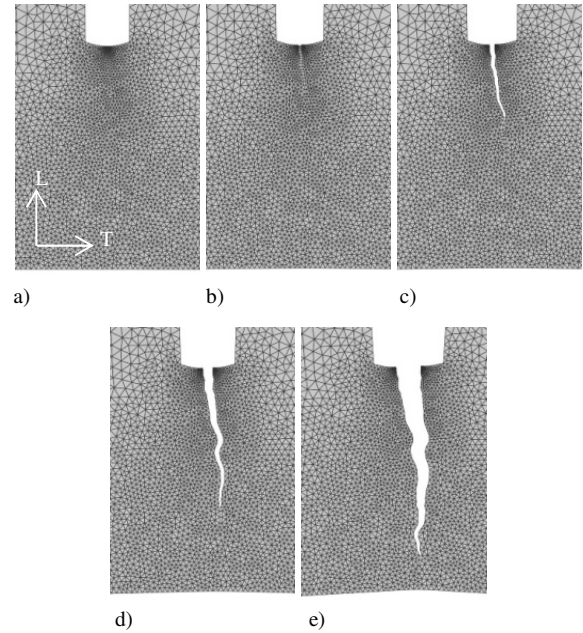


Figure 12: Fracture path from the numerical simulation of the small orthotropic sample with a TL crack starting at the imperfection. a) Elastic response. b) Crack initiation. c) Transition from crack initiation to propagation. d) Crack propagation. e) Ultimate failure.

ACKNOWLEDGEMENT

This work is part of the research programme Science4Arts, which is financed by the Netherlands Organisation for Scientific Research (NWO). The authors acknowledge the helpful discussions with S.E. Ekelund (Eindhoven University of Technology (TU/e) / Rijksmuseum Amsterdam), P.H.J.C. van Duin (Rijksmuseum Amsterdam), H.A. Ankersmit (Cultural Heritage Agency of the Netherlands) and R.M. Groves (Delft University of Technology) on topics related to the fields of conservation, cultural heritage and experimental mechanics. The authors appreciate the assistance of S.E. Ekelund (TU/e), S. Segers (TU/e) and H.L.M. Wijen (TU/e) during the performance of the experimental tests, and the help of T. Arends (TU/e), J.H.J. Dalderop (TU/e) and I. Joosten (Cultural Heritage Agency of the Netherlands) in taking SEM photographs. The authors also appreciate the helpful discussion with R.K.W.M. Klaassen (Stichting Hout Research) on oak wood anatomy.

REFERENCES

- [1] S. Ekelund, P. van Duin, A. Jorissen, B. Ankersmit. A method for studying changes on decorated oak wooden panels. (submitted).
- [2] M.V. Cid Alfaro, A.S.J. Suiker, R. De Borst, J.J.C. Remmers. Analysis of fracture and delamination in laminates using 3D numerical modelling. *Engineering Fracture Mechanics*, 76:761-780, 2009.
- [3] X.P. Xu, A. Needleman. Numerical simulations of fast crack growth in brittle solids. *Journal of the Mechanics and Physics of Solids*, 42(9):1397-1434, 1994.

- [4] E.N. Landis, S. Vasic, W.G. Davids, P. Parrod. Coupled experiments and simulation of microstructural damage in wood. *Experimental Mechanics*, 42(4):389-394, 2002.
- [5] S. Saft, M. Kaliske. A hybrid interface-element for the simulation of moisture-induced cracks in wood. *Engineering Fracture Mechanics*, 102:32-50, 2013.
- [6] L.P. Qiu, E.C. Zhu, J.W.G. van der Kuilen. Modeling crack propagation in wood by extended finite element method. *European Journal of Wood and Wood Products*, 72:273-283, 2014.
- [7] Nordtest. Wood: fracture energy in tension perpendicular to the grain NT BUILD 422. Nordtest, Espoo, 1993.
- [8] International Organisation for Standardization (ISO): Wood – Determination of moisture content for physical and mechanical tests. ISO, Switzerland, 1975.
- [9] Abaqus 6.13-2. Abaqus 6.13-2 Documentation. Dassault Systèmes Simulia Corp., U.S.A. Providence RI, 2013.
- [10] M.G.A. Tijssens, E. Van Der Giessen, L.J. Sluys. Simulation of mode I crack growth in polymers by crazing. *International Journal of Solids and Structures*, 37:7307-7327, 2001.
- [11] M.V. Cid Alfaro, A.S.J. Suiker, R. De Borst. Transverse failure behaviour of fiber-epoxy systems. *Journal of Composite Materials*, 44(12):1493-1516, 2010.
- [12] M.V. Cid Alfaro, A.S.J. Suiker, C.V. Verhoosel, R. De Borst. Numerical homogenization of cracking processes in thin fibre-epoxy layers. *European Journal of Mechanics A/Solids*, 29:119-131, 2010.
- [13] R.A. Luimes, A.S.J. Suiker, A.J.M. Jorissen, H.L. Schellen. Fracture behaviour of historic oak wood under three-point bending – an experimental-numerical study. In: Analysis and characterisation of wooden cultural heritage by scientific engineering methods, 51-62, 2016.
- [14] Z. P. Bazant. Size effect. *International Journal of Solids and Structures*, 37:69-80, 2000.